metals

MDPI

Article

Bonding and Stability of Ternary Structures in the CeT_2Al_{20} (T=Ta, W, Re) and YRe_2Al_{20} Alloys

Gili Yaniv, Daniel Vidal, David Fuks and Louisa Meshi *

Department of Materials Engineering, Ben Gurion University of the Negev, POB 653, Beer Sheva, Israel; gilisha@post.bgu.ac.il (G.Y.); vidald@post.bgu.ac.il (D.V.); fuks@bgu.ac.il (D.F.)
* Correspondence: louisa@bgu.ac.il; Tel.: +972-8-6472576

Received: 12 March 2020; Accepted: 24 March 2020; Published: 25 March 2020

Abstract: A-T-Al aluminides, where A = actinide, lanthanide or rare earth elements and T = transition metals, have attracted considerable attention as potential materials where heavy fermions may be formed. This led to the discovery of superconducting properties in cubic AT_2Al_{20} compounds with $CeCr_2Al_{20}$-type crystal structure. Other Al-rich aluminides, belonging to these A-T-Al systems, exhibited different physical properties as a function of their crystal structure. Thus, predicting the stable structure of the Al-richest phase that will form in the A-T-Al systems is highly valuable. Stability of the crystal structures, forming in the CeT_2Al_{20} and YRe_2Al_{20} systems, was studied in current research using density functional theory (DFT) calculations. It is demonstrated that the total spin magnetic moment of the transition metal can be used as a descriptor for phase stability assessment in the AT_2Al_{20} systems, where T is a 5*d* transition metal. Basing on crystallographic considerations, degree of distortion of the coordination polyhedrons, formed around T atoms, can be directly connected to the specific type of structure crystallizing in these systems.

Keywords: density functional theory; aluminides; electronic structure; stability

1. Introduction

A-T-Al family of alloys (where A = actinides, lanthanides or rare earth elements; T = transition metals) was extensively studied, due to its ability to form heavy fermions [1–12]. In theory, there are hundreds of possible ternary Al-rich A-T-Al phases which can form in these systems, but in reality all these phases can be classified into only a handful of structure types, such as tetragonal AT_xAl_{12-x} ($ThMn_{12}$ type) [4,13], tetragonal AT_2Al_{10} ($CaCr_2Al_{10}$ type) [14], orthorhombic AT_2Al_{10} ($YbFe_2Al_{10}$ type) [15] and cubic AT_2Al_{20} ($CeCr_2Al_{20}$ type) [16], see Table 1. For illustration, unit cells of these structures are shown in Figure 1. In fact, the amount of possible structures forming in these systems is even less than listed here since tetragonal AT_2Al_{10} ($CaCr_2Al_{10}$ type) and orthorhombic AT_2Al_{10} ($YbFe_2Al_{10}$ type) were declared as structural derivatives of the tetragonal AT_xAl_{12-x} ($ThMn_{12}$ type) [17].

Cubic AT_2Al_{20} structure is of particular importance since phases of this type exhibited unique physical properties [18,19]. The unit cell of the AT_2Al_{20} structure ($CeCr_2Al_{20}$-type) may be presented as a packing of coordination polyhedrons formed around heavy atoms. Around A-type atoms a polyhedron with 16 vertices occupied by Al atoms exists. Such polyhedron is of Frank-Kasper type [20]. Since the shortest A-A atomic distance is about 6Å, the A atoms are considered to be isolated from each other, and the structure can be classified as cage-type [18]. In addition to the AT_2Al_{20}, there are other structures classified as a cage-type, for example: the filled skutterudites [21] and the Laves phases [22]. In these systems, low-energy, large amplitude, localized anharmonic vibrations of cage-filling atoms are observed. This "rattling" of atoms affects thermal and transport properties of materials. It is believed that superconducting critical temperature, T_c is enhanced by this effect in different cage-type structures, among them are $CeCr_2Al_{20}$-type compounds. For example, PrT_2Al_{20} (T = Ti, V) are exotic

superconductors in which the superconducting state coexists with the quadrupolar ordering [19]. Superconductivity behavior was also found in RV_2Al_{20} (R = Sc, Y, Lu) compounds, where LuV_2Al_{20} exhibited critical temperature T_c = 0.6 K [18]. By introducing elements with 4*f*-/5*f*-electrons into the 8*a* position of a $CeCr_2Al_{20}$-type structure, variety of additional magnetic properties can be promoted. Antiferromagnetic ordering is one of these properties, documented in several AT_2Al_{20} systems, e.g., in SmT_2Al_{20} and $GdTi_2Al_{20}$ (where T = Ti, V and Cr) [23]. YbT_2Al_{20} (T = Ti, V, Cr) are Pauli paramagnets with a divalent Yb ion [24] and NdT_2Al_{20} (T = V,Cr) are ferromagnets [25].

The discovery of new phases that could possess such unique attributes is mainly performed by tedious "trial and error approaches". In [26–28], an extensive research was reported which was undertaken with the purpose to formulate a rule that will allow the prediction of the stable structures formed in this family of alloys. First steps towards achieving this goal were made in [27]. Keeping the A atom constant (A = Th) and changing 3*d* transitional metals (T = Ti, V, Cr, Mn and Fe), the influence of 3*d* transitional metals on the stability of the phases, crystalizing in ThT_2Al_{20} alloys, was studied. It was found that stability of the structure formed in the ThT_2Al_{20} systems is determined by the minimal value of magnetic moment of transition metal. This understanding was expanded in [28], where the role of A elements on the formation of the stable ternary Al-rich phases, crystallizing in the AMn_2Al_{20} alloys, was discussed. Mn was chosen as a representative of a *3d* transition metal since it was found to be the breakage point of symmetry. It was demonstrated that the rule suggested in [27] is satisfied if A element is lanthanide/rare earth with 4*f*-electrons/no *f*-electrons in the shells beyond the totally filled inert gas shell. Otherwise, i.e., if A has 5*f*-electrons, the average energy of 3*d*-electrons of the transition metal should be used as a descriptor for assessment of the stability of the structure [28]. It was also shown that the reason for this different behavior is due to the fact that 4*f*-electrons are almost not excited by the crystal field, and they do not participate in the bonding with 3*d*-states of T. On the other hand, 5*f*-orbitals form a relatively wide band and participate in the bonding with the 3*d*-orbitals. Furthermore, when such *f*-*d* hybridization becomes significant, the stable structure will be the one with the minimal average energy of *3d*-electrons of the transition metal.

Such fine interplay between the bonding tendencies of 4*f*- or 5*f*-electrons of rare earth/lanthanides atoms with 3*d*-electrons of transition metals stimulated current research, aiming to understand the stability of similar Al-rich ternary phases (in the A-T-Al systems) with transition metals containing 5*d*-electrons. This is not a trivial task, since the role of 5*d*-electrons in the stabilization of the structure may differ, as compared with the similar ternary phases, where T=3*d* transition metal. 5*d*-electrons are more delocalized in the background of the surrounding atoms in the A-T-Al compounds, due to the shielding effect that occurs because of screening of the part of 5*d*-electrons density by internal 4*f*-orbitals of transition metals.

In current research, it was of interest to check the validity of formulated earlier rules governing the stabilization of ternary Al-rich A-T-Al structures of compounds with T=3*d* transition metals for the same compounds with T = 5*d* transition metal. It should be noted that 4*d* transition metals could not be studied since Tc (which is at the same column in the periodic table as symmetry breaking element Mn) is a radioactive material and, therefore, calculation results could not be compared with experimental ones.

In order to understand the stability of the structures formed in the AT_2Al_{20} alloys, where T are from the 5*d* transition metals row, Ce-T-Al (T = Ta, W and Re) and Y-Re-Al systems were studied using density functional theory (DFT). It is interesting to note that amount of possible structure types with the AT_2Al_{10} stoichiometry increases when T=Re. With T=3*d* transition metals, only orthorhombic ($YbFe_2Al_{10}$-type) and tetragonal ($CaCr_2Al_{10}$-type) structures exist. With T = Re, several additional structural derivatives of the orthorhombic ($YbFe_2Al_{10}$-type) structure were reported as having double and triple *c* lattice parameter of the $YbFe_2Al_{10}$-structure type. These derivatives has $TbRe_2Al_{10}$ (Figure 1e) and the $LuRe_2Al_{10}$ (Figure 1f) structure types, respectively [29,30] (see Table 1 for crystallographic details). Moreover, Re is a special case since it is situated in the same column as Mn in the periodic table and, thus, might be also a point of symmetry breakage, following the

theory developed in [27,28]. This hypothesis can be demonstrated in Figure 2, presenting the reported structures that are formed in the Al-rich A-T-Al systems (where T = 5*d* transition metals). It is clear from this table that when T = W and Ta, cubic phases are formed in the AT_2Al_{20} alloys with essentially all A-type elements. When T = Re, the symmetry breaks, and the phases do not crystalize in the cubic symmetry. The novelty of current work is the demonstration of the ability to predict the stable structure of complex ternary Al-rich compounds in the A-T-Al systems where T = 5*d* transition metals. For the first time crystallographic analysis is presented, connecting the degree of distortion of coordination polyhedron formed around the transition metal and the specific crystal structure formed.

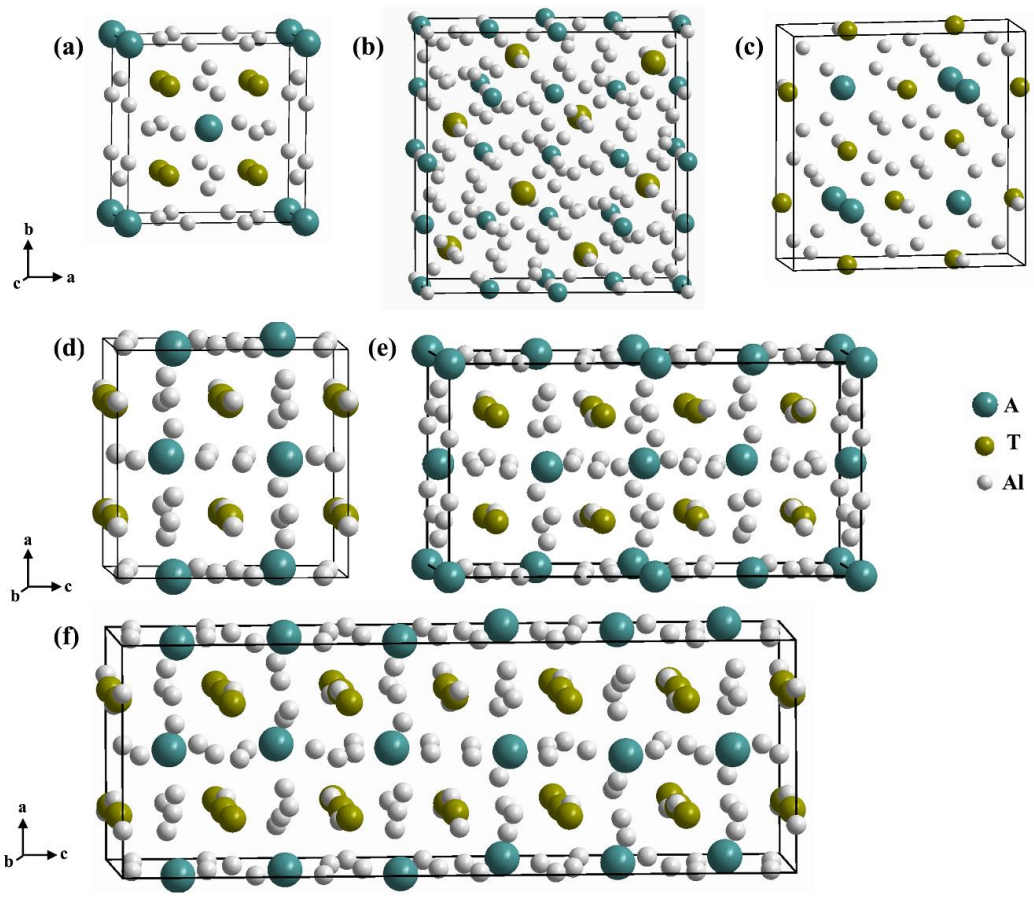

Figure 1. Unit cell representation of the discussed structures: (**a**) tetragonal, AT_xAl_{12-x} ($ThMn_{12}$-type); (**b**) cubic, AT_2Al_{20} ($CeCr_2Al_{20}$-type); (**c**) tetragonal, AT_2Al_{10} ($CaCr_2Al_{10}$-type); (**d**) orthorhombic, AT_2Al_{10} ($YbFe_2Al_{10}$–type); (**e**) orthorhombic 2*c*, AT_2Al_{10} ($TbRe_2Al_{10}$–type); (**f**) orthorhombic 3*c*, AT_2Al_{10} ($LuRe_2Al_{10}$–type). The unit cell were visualized using Diamond commercial software.

Table 1. Crystallographic parameters of the Al-richest A-T-Al structures.

Geometry and Stoichiometry	Structure Type	Space Group	Representative Structure	Lattice Parameters Å
Tetragonal, AT_xAl_{12-x}	$ThMn_{12}$	I4/*mmm*	UFe_4Al_8	*a* = 8.749 *c* = 5.036 [4]
Cubic, AT_2Al_{20}	$CeCr_2Al_{20}$	$Fd\bar{3}m$	CeV_2Al_{20}	*a* = 14.558 [31]
Tetragonal, AT_2Al_{10}	$CaCr_2Al_{10}$	P4/*mnm*	$GdMn_2Al_{10}$	*a* = 12.733 *c* = 5.128 [32]
Orthorhombic, AT_2Al_{10}	$YbFe_2Al_{10}$	C*mcm*	$YbFe_2Al_{10}$	*a* = 8.966 *b* = 10.153 *c* = 9.003 [15]
Orthorhombic 2c, AT_2Al_{10}	$TbRe_2Al_{10}$	C*mcm*	$TbRe_2Al_{10}$	*a* = 9.322 *b* = 10.304 *c* = 18.032 [33]
Orthorhombic 3c, AT_2Al_{10}	$LuRe_2Al_{10}$	C*mcm*	$LuRe_2Al_{10}$	*a* = 9.291 *b* = 10.277 *c* = 26.841 [29]

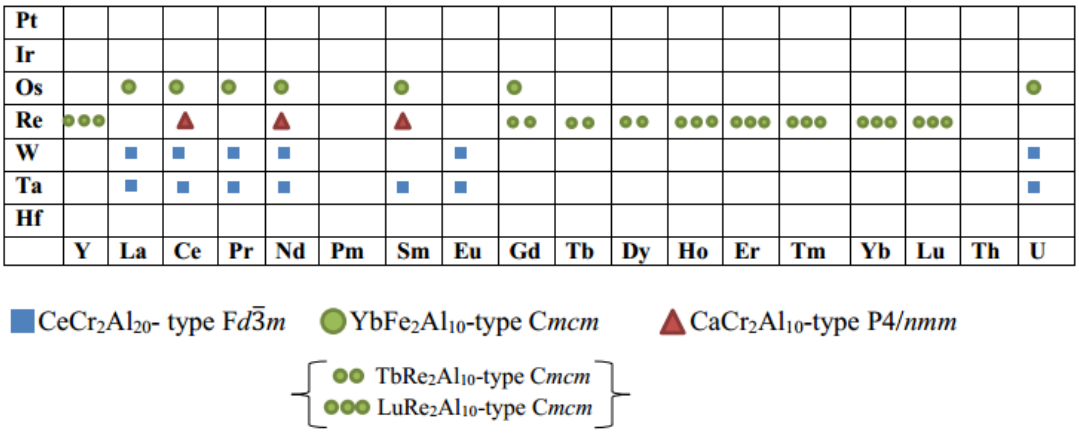

Figure 2. Summary of the reported A-T-Al phases with AT_2Al_{20} and AT_2Al_{10} compositions containing 5*d* T metal. Different symbols present various symmetries according to the legend presented below the table. The symbols demonstrate the crystal structure of the phase in a specific system. The data are from [34].

2. Materials and Methods

DFT calculations were performed in the framework of the Full Potential + Linearized Augmented Plane Wave (FP-LAPW) method [35]. These calculations allow analysis of the relative stability of structures of considered phases. Total energy spin-polarized calculations of competing phases were performed. In this work spin orbit coupling (SOC) calculations were carried out as well since here, unlike previous work [27,28] the transition metal, Re, is much heavier than 3*d* transition metals. The results are presented with and without SOC calculations. WIEN2k code (Version 10.1) [36] was applied for calculations. In this code, the core states are treated as fully relativistic [36] and the valence states are considered using a scalar relativistic approach [37].

Since the studied systems contain lanthanides and rare earth elements, the exchange correlation effects should be carefully examined. The exchange-correlation potential was calculated within the Perdew–Burke–Ernzerhof (PBE) generalized gradient approximation (GGA) [38]. The application of hybrid density functional theory method (HYB-DFT) [39,40] to similar systems with *3d*-metals was discussed in [28], where HYB-DFT calculations were performed by the "exact exchange for correlated electrons" method. The hybrid functional replaces a fraction of DFT exchange with exact Hartree–Fock (HF) exchange and applied only to a selected set of lanthanides" or actinides" electrons, namely the 4*f*- or 5*f*- electrons inside the atomic sphere. The hybrid exchange-correlation energy functional $E_{xc}^{PBE+\alpha HF}$ has the form [41]:

$$E_{xc}^{PBE+\alpha HF} = \alpha E_x^{HF} + (1-\alpha)E_x^{PBE} + E_c^{PBE} \quad (1)$$

where E_x^{HF} is the HF exchange, E_x^{PBE} is the PBE exchange functional and E_c^{PBE} is the PBE correlation functional. The mixing parameter α denotes the fraction of HF exchange replacing the PBE exchange. It has been shown that by increasing the amount of HF exchange, one increases the degree of electronic localization. It was also demonstrated that PBE nicely reproduces the stability of crystal structures for all considered systems and gives the results similar to HYB-DFT for all studied systems when α = 0.05. Larger magnitudes of α do not describe this phase competition in a correct way. It should be mentioned that nowadays also DFT plus Hubbard U (DFT + U) method is widely used for strongly correlated systems. In this approach, an orbital dependent field is introduced providing a correction for the self-interaction [42]. DFT + U significantly improve the results for band gap, optic, X-ray absorption or magnetic properties for insulating actinide oxides (such as UO_2), for oxides where the charge ordering is observed [43,44], and for some bromides (see, for example [45]). The detailed examination of the LDA + U method in the framework of a plane-wave pseudopotential approach may be found in [46].

We decided not to use this approach here for several reasons: (a) the Coulomb parameter, U, and exchange parameter, J, determined by first principle calculations do not always give reliable results for some Fe-based compounds (as an example) [47]; (b) our own experience [27,28,48,49] shows that the DFT in the GGA approximation with PBE functional very well reproduces the basic structural and electron spectrum properties of U- and Th-based binary, ternary and even quaternary compounds; (c) recent results [50–52] have demonstrated that DFT + U approach is not necessary for a correct description of U metal and mixing energies in the U-based compounds; (d) we consider the total energy differences to estimate the relative stability of compounds. In this case, possible GGA inaccuracies are canceled as it was demonstrated in [53].

The details of our calculations are following: the used muffin-tin radii (R_{MT}) were equal to 2.5 Bohr for all atoms (Ta, W, Re, Y and Ce) except Al, for which R_{MT} was chosen equal to 2.2 Bohr. This choice is dictated by the necessary condition to avoid overlapping between the atomic spheres in the volume optimization procedure. For the basis-set size at each point, the cut-off parameters $R_{MT}K_{max} = 7$ was used, where K_{max} is the magnitude of the largest k vector in the wave function expansion. A maximum l, l_{max}, equal to 10 was taken in the expansion of the radial wave functions inside the atomic sphere to represent the valence states. The cut-off energy, separating core and valence states was chosen to be equal to −7.0 Ryd for all atoms. This condition is necessary for minimization of leakage of the electron core states into the interstitial region. All integrations over the Brillouin zone (BZ) were done using TEMPS scheme implemented in WIEN2k with the broadening parameter in Fermi energy calculations equal to 0.002 that corresponds to ~40 °C. It was found that the number of k-points in the first BZ equal to 300 is enough to obtain the accuracy of the self-consistent calculations for the energy of the system not less than ~10^{-3} Ryd. It should be noted that for the Ce-Re-Al system, energies were calculated with higher accuracy (~10^{-4} Ryd), due to the fact that energy differences between competing structures are smaller than 10^{-3} Ryd. Keeping in mind that the stability of the structure is determined by comparison of the energies of structures in equilibrium conditions, volume optimization was carried out for each structure aiming at minimal total energy determination. Using a set of energies and corresponding volumes of the unit cells, the equilibrium volume of the unit cell of all considered phases was obtained by fitting the data to Murnaghan equation of state [54]. The total energies of the competing structures of the phases were compared for the optimized structures. Such procedure not only allows confirmation of the stability of experimentally observed structures but also gives possibility to compare experimental and theoretical lattice parameters of the observed structures, providing an opportunity to assess the quality of calculations.

3. Results and Discussion

In the current research, the hypothesis of structure stability, suggested in [27,28], was checked for the row of 5*d* transition metals. Ce with electron configuration of $[Xe]4f^1 5d^1 6s^2$ was chosen as representative of the A atom type in the studied AT_2Al_{20} composition and the 5*d* transition metals changed from Ta to Re. A = Y was chosen due to its different than Ce electron configuration, i.e., $[Kr]\ 4d^1 5s^2$, without *f*-electrons in its outer shell.

DFT calculations were performed for the CeT_2Al_{20} alloys (with T = Ta, W) considering three main structures types: cubic ($CeCr_2Al_{20}$-type), tetragonal ($CaCr_2Al_{10}$–type) and orthorhombic ($YbFe_2Al_{10}$-type). In addition, since for T = Re different structural derivatives of the orthorhombic ($YbFe_2Al_{10}$-type) structure exist (see Table 1), calculations for the ARe_2Al_{20} alloys (A = Ce, Y) were also carried out for the doubled $YbFe_2Al_{10}$-type *c* lattice parameter (2*c*) ($TbRe_2Al_{10}$-type) and tripled *c* $YbFe_2Al_{10}$-type lattice parameter (3*c*) ($LuRe_2Al_{10}$-type) unit cells. Due to the existence of these two structural derivatives, disordered orthorhombic ($YbFe_2Al_{10}$-type) is regarded later on as 1*c*.

Comparing the minimal energies of the competing structures is not a trivial task since the number of atoms in each structure should be taken into account. DFT calculations are performed for the unit cells rather than for the conventional lattice cells, therefore, transferring from conventional lattice cell to

a unit cell reduces the number of atoms for the orthorhombic structure (1*c*) and its structural derivatives (2*c* and 3*c*) by two and for the cubic structure by four. The tetragonal unit cell will remain unchanged.

It can be understood from Table 2 that the total number of atoms in the tetragonal unit cell is twice the number of atoms containing the orthorhombic 1*c* structure. Thus, in order to compare the minimal energies for these structures, the total energy of the tetragonal structure should be divided by 2. Similarly, the total energies of the orthorhombic 2*c* and 3*c* should be divided by 2 or 3, respectively.

Table 2. Total number of each type of atoms in the conventional lattice cell (denoted by the space group notation) and in the corresponding unit cell used for the density functional theory (DFT) calculations. Orthorhombic structure is referred by "Ortho".

Phase	Cubic		Tetragonal		Ortho 1*c*		Ortho 2*c*		Ortho 3*c*		Pure Al	
Cell Type	$Fd\bar{3}m$	Unit Cell	$P4/nmm$	Unit Cell	$Cmcm$	Unit Cell	$Cmcm$	Unit Cell	$Cmcm$	Unit Cell	$Fm\bar{3}m$	Unit Cell
Total number of atoms	184	46	52	52	52	26	104	52	156	78	4	1
A atoms	8	2	4	4	4	2	8	4	12	6	0	0
T atoms	16	4	8	8	8	4	16	8	24	12	0	0
Al atoms	160	40	40	40	40	20	80	40	120	60	4	1

Since the cubic structure crystalizes in the AT_2Al_{20} composition while all other structures possess AT_2Al_{10} composition, the excess of pure Al atoms that obtained experimentally (in [26–28], for example), should be accounted when the relative stability of these phases is considered. The cubic structure has 20 Al atoms more than the other structures. Therefore, the formation energy of pure Al-metal structure (FCC), multiplied by 20, should be added to both tetragonal and orthorhombic structures to keep the composition constant. The calculated total energy for pure Al at equilibrium volume per atom was found to be equal to −485.646 Ry. In order to obtain the energy preference of one structure over the other the following equation should be used:

$$\Delta E = \left(E_{AT_2Al_{10}} + 20 \cdot E_{Al,\ \ Fm3m}\right) - E_{AT_2Al_{20},\ \ Fd\bar{3}m} \tag{2}$$

The energy differences for all competing structures for the Ce-T-Al and Y-Re-Al systems at AT_2Al_{20} composition are presented in Table 3, with and without SOC calculations. For the Re based systems, calculations of the structural derivatives are also presented. ΔE shows the preference of the structure with respect to the cubic one, i.e., more negative ΔE value points on more stable structure. It can be seen that the cubic structure is preferred in the $CeTa_2Al_{20}$ and CeW_2Al_{20} alloys. In the $CeRe_2Al_{20}$ alloy, breakage of symmetry occurred and the tetragonal structure was found to be the stable one. When the A atom type is Y, the orthorhombic 3*c* structure is stable. Results of calculations were compared with the experimental data [1,55–57]. In the CeT_2Al_{20} (T = Ta and W) systems, the stable structure was determined as cubic (i.e., $CeCr_2Al_{20}$ type), while for the $CeRe_2Al_{20}$ and YRe_2Al_{20} alloys the stable structures of the Al-richest ternary phases were found to be tetragonal ($CaCr_2Al_{10}$ type) and orthorhombic 3*c* ($LuRe_2Al_{10}$-type), respectively. As mentioned, our results presume additional pure Al phase in these two alloys to preserve studied here AT_2Al_{20} composition. Table 4 presents the comparison of the experimental unit cell parameters, as reported in the literature and the values retrieved from the calculations. The results are in excellent agreement.

According to [28], the value of the magnetic moment of the transition metal may be used to predict the stable structure of the ternary Al-rich phase that will form in the AT_2Al_{20} alloys (where T = 3*d* transition metals and A = lanthanide with 4*f* electron or no *f* electrons in theirs shells beyond the totally filled inert gas shell). Minimal value of the magnetic moment corresponds to a large splitting between the e_g and t_{2g} states due to the fact that majority of 3*d*-electrons occupy the lowest energy levels. According to the Theory of Coordination Compounds (TCC) [58], the large splitting between the e_g and t_{2g} energies corresponds to a strong crystal field of the transition metal neighborhood and, thus, to a more stable structure. It should be noted that this "rule" was applied to AT_2Al_{20} alloys where

A was either with 4*f*-electrons that are well localized or without *f*-electrons in the outer shell, therefore, spectroscopic and magnetic properties were independent of the environment [28].

Table 3. Energy differences, ΔE(Ryd), with respect to the cubic structure.

System	Structure	ΔE without SOC	ΔE with SOC
Ce-Ta-Al	Cubic	0	0
	Tetragonal	0.206	0.310
	Orthorhombic 1*c*	0.351	0.457
Ce-W-Al	Cubic	0	0
	Tetragonal	0.043	0.036
	Orthorhombic 1*c*	0.131	0.124
Ce-Re-Al[1]	Cubic	0	0
	Tetragonal	−0.1469	−0.2897
	Orthorhombic 1*c*	−0.1447	−0.2876
	Orthorhombic 2*c*	−0.144	−0.286
	Orthorhombic 3*c*	−0.142	−0.283
Y-Re-Al	Cubic	0	0
	Tetragonal	−0.242	−0.242
	Orthorhombic 1*c*	−0.212	−0.213
	Orthorhombic 2*c*	−0.240	−0.240
	Orthorhombic 3*c*	−0.246	−0.246

[1] It should be noted that due to very small energy differences obtained for the tetragonal and orthorhombic 1*c* structures in the Ce-Re-Al system, total energies of these structures were calculated up to accuracy ~10^{-4}Ry for corresponding unit cells.

Table 4. Lattice parameters for the stable phases, in Å.

Phase	DFT Calculations	Experimental Results
$CeTa_2Al_{20}$	a = 14.787	a = 14.748 [1]
CeW_2Al_{20}	a = 14.647	a = 14.589 [57]
$CeRe_2Al_{10}$	a = 12.955 c = 5.198	a = 12.956 c = 5.172 [55]
YRe_2Al_{10}	a = 9.337 b = 10.342 c = 27.026	a = 9.306 b = 10.308 c = 26.936 [56]

Calculated magnetic moments of the 5*d* transition metals, in studied here systems for each competing structure, are presented in Table 5. The behavior of the magnetic moments of the 5*d* transition metals complies with suggested for the 3*d* transition metals theory. It can be seen that the lowest value of the magnetic moment corresponds to the stable structure formed in each system. For the CeT_2Al_{20} (T = Ta, W), the lowest value is obtained for the cubic structure, while when T = Re the tetragonal structure possesses the lowest value. For the YRe_2Al_{20} alloy, even if we sum up the magnetic moments of both Re (1) and Re (2) type atoms, the orthorhombic 3*c* structure has the lowest value of magnetic moment of Re, see Table 5. It should be noted that in all other discussed structures, besides orthorhombic 3*c*, transition metal occupies only one Wyckoff site, marked as Re (1) in Table 5.

Confirmation of the fact that *f*-electrons do not influence the stability trends in considered systems may be found through the analysis of Density of States (DOS) for electrons. As an example, the calculated local partial DOS for the 4*f*-states of Ce and 5*d*-states of Re are presented in Figure 3 for three main competing structures (i.e., cubic, tetragonal and orthorhombic 1*c*). The 4*f* electrons peak of Ce is localized above the Fermi energy level. These electrons do not contribute to the bonding with 5*d* electrons of Re. For the studied here Y-based compounds similar analysis of partial DOS (not presented here) has shown that only small amount of promoted Y *f*-states in the background of the rest of atoms exists, and they also do not influence the competition between the structures. Thus, the 4*f* electrons of Ce and promoted *f*-states of Y do not influence the structure stability. This conclusion underlines that

the magnetic moment of the transition metal can be used as a descriptor to predict the stable Al-rich ternary structure that will form in the AT_2Al_{20} alloys when T is 3*d* or 5*d* transition metal.

Table 5. Magnetic moment (in μB) of the transition metal in the considered structures in the CeT_2Al_{20} (T=Ta, W, Re) and YRe_2Al_{20} alloys.

Studied Systems		Main Structures			Structural Derivatives	
System type	**T atom**	**Cubic**	**Tetragonal**	**Orthorhombic 1*c***	**Orthorhombic 2*c***	**Orthorhombic 3*c***
Ce-Ta-Al	Ta	0.00701	0.00854	0.01025	-	-
Ce-W-Al	W	0.00937	0.01867	0.01182	-	-
Ce-Re-Al	Re(1)	0.00743	0.00123	0.00288	0.00830	0.00744
	Re(2)	-	-	-	-	0.00796
Y-Re-Al	Re(1)	0.00530	0.00031	0.00259	0.00049	0.00015
	Re(2)	-	-	-	-	0.00006

Since magnetic moment of T atom type is the one which dictates the stability, coordination polyhedron formed around this atom in each structure should dictate the geometry of the structure (i.e., cubic, tetragonal or orthorhombic). The difference between the discussed here structures can be expressed in terms of distortion of the coordination polyhedron formed around T, and might also effect the stability according to the Jahn-Teller effect and TCC theory [58,59]. In all structures discussed in this manuscript (including their structural derivatives), icosahedron (with coordination 12) is formed around T atoms. In cubic structure (of the $CeCr_2Al_{20}$ type), this icosahedron is the closest to perfect one because only Al atoms occupy its vertices. Although these Al atoms belong to two different Wyckoff positions, the distances from the center of the icosahedron (occupied by the T atom) to its vertices are almost equal, see Table 6. In other structures discussed in this manuscript, icosahedrons formed around T atoms contain two A-type atoms and 10 Al atoms, as shown in Table 6, thus, they are distorted. Degree of polyhedral distortion was calculated following [60] and is presented in Table 6. According to [60], the volume of icosahedron is equal to $2.5362r^3$, where r denotes the center-to-vertex distance for a regular/ideal polyhedron. The polyhedral distortion was calculated as follows:

$$v(\%) = (V_i\text{-}V_r)/V_i \times 100 \quad (3)$$

where V_i is the volume of the ideal icosahedron (which belong to the cubic structure in our case), and V_r is the volume of the regular icosahedron. It should be noted that out of all reported in the database [34] representatives of the discussed structure types we have chosen for comparison T and A atom types with similar atomic radius, since identical atoms do not form all these structures, as discussed here and in our previous publications [17,26–28]. It can be clearly seen that in each structure the degree of polyhedral distortion is different with tetragonal structure having the highest degree of distortion relatively to the orthorhombic ones. Combining this understanding with the above made conclusion it can be proposed that the magnetic moment of the T atom imposes the required degree of distortion of the polyhedron which as a result will impose the geometry of the unit cell (i.e., highest distortion-tetragonal, smaller distortion-orthorhombic and zero distortion-cubic). For differentiation between three possible orthorhombic structures (1*c*, 2*c*, 3*c*), crystallographic analysis should be extended.

In Figure 4, chains of interconnected icosahedrons, as formed in the unit cells of three orthorhombic structures, are presented. In the 1*c* orthorhombic structure, T and A atom types occupy one Wyckoff position each. Thus, icosahedrons, connected through the vertices occupied by the A type atoms, form parallel to *c* direction rows, see Figure 4a. In the 2*c* orthorhombic structure, T atom occupies one Wyckoff position and A atom occupies two different Wyckoff positions—thus there are two independent options to interconnect these icosahedrons. Consequently, icosahedrons form zigzag-like chains along the same *c* direction, as shown in Figure 4b. In the 3*c* orthorhombic structure, both T and A atoms occupy two independent Wyckoff positions. Around one position, icosahedron is formed exactly as in the 1*c* structure, i.e., it includes two A atoms occupying the same Wyckoff site, see Re (2) in

Table 6. Thus, such icosahedrons form straight row with their neighboring icosahedrons. The second position of T atom (Re (1) in Table 6) is surrounded by the same, as in the 2*c* structure, icosahedra (with A-type atoms at two different Wyckoff positions) which imposes it to interconnect in a zigzag shape. Thus, in this structure both rows and zigzags exist, imposing larger unit cell, see Figure 4c. Variety in the sequence of the coordination icosahedra provide an opportunity to have several derivatives of the orthorhombic structure as a function of degree of distortion imposed by the T and A atom types.

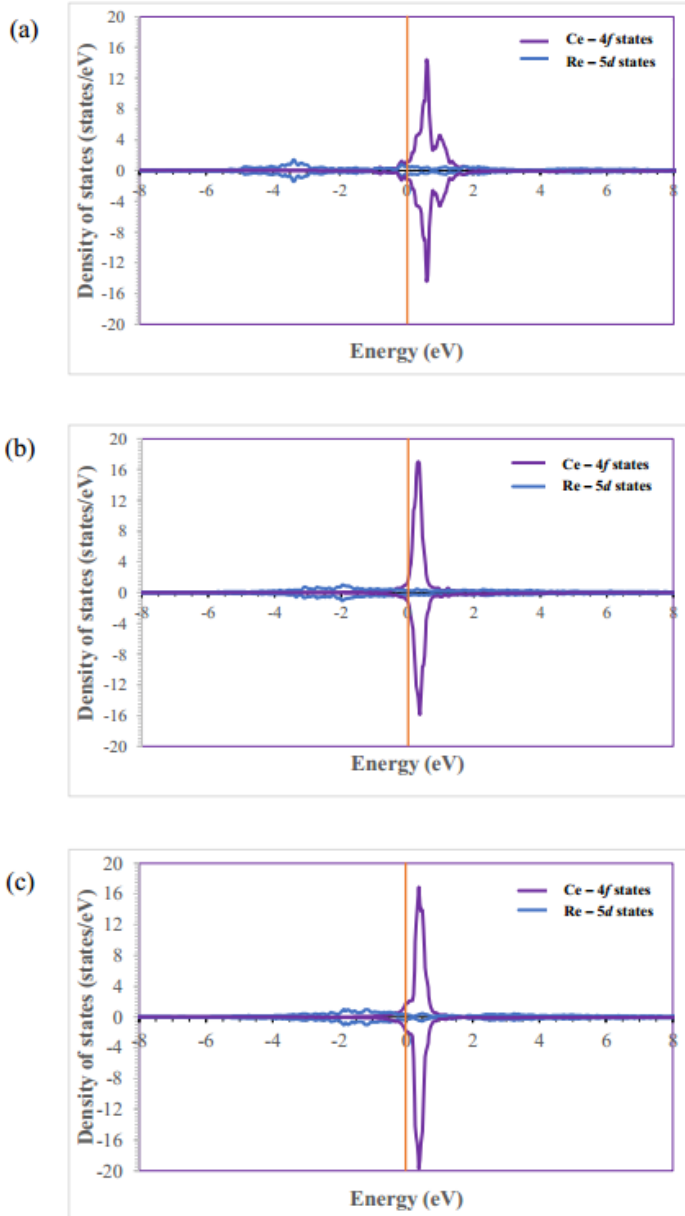

Figure 3. Partial Density of States (DOS) for 4*f*-states of C*e* and 5*d*-states of Re for the $CeRe_2Al_{20}$ alloy calculated for the competed structures: (**a**) cubic; (**b**) tetragonal; (**c**) orthorhombic 1*c*. Fermi energy is set to zero.

Summarizing, it can be proposed that in the A-T-Al systems (where A-type atoms have 4f electrons or no f-electrons in the outer shell) the stability of the Al-richest ternary phase can be predicted by the magnetic moment of the T atom. In fact, this parameter prognosticates the degree of distortion of the coordination polyhedron formed around T atom which stabilizes the structure. When the needed distortion is achieved, the geometry of the unit cell is set following the interconnection of the icosahedrons formed around the T atom types.

Table 6. Calculation of the degree of distortion of the icosahedron formed around T atom in the discussed structures. Following [60], r parameter is the average distance from the center to the vertices of the coordination polyhedron. Distances are given in Å. For calculations, atomic models of $EuTa_2Al_{20}$, $NdRe_2Al_{10}$, $LnOs_2Al_{10}$, $GdRe_2Al_{10}$ and YRe_2Al_{10} (taken from [34]) were used as prototypes of cubic, tetragonal and 1*c*, 2*c*, 3*c* orthorhombic structures, respectively, containing A and 5*d* T atoms.

Parameters	Cubic ($EuTa_2Al_{20}$)	Tetragonal ($NdRe_2Al_{10}$)	Ortho 1*c* ($LnOs_2Al_{10}$)	Ortho 2*c* ($GdRe_2Al_{10}$)	Ortho 3*c* (YRe_2Al_{10})	
T atom type	Ta	Re	Os	Re	Re(1)	Re(2)
Vertex 1	Al 2.624	Al 2.5721	Al 2.591	Al 2.5474	Al 2.5389	Al 2.5679
Vertex 2	Al 2.624	Al 2.5721	Al 2.591	Al 2.6017	Al 2.5967	Al 2.5679
Vertex 3	Al 2.624	Al 2.5945	Al 2.578	Al 2.6021	Al 2.6071	Al 2.6096
Vertex 4	Al 2.624	Al 2.6044	Al 2.578	Al 2.6127	Al 2.6212	Al 2.6096
Vertex 5	Al 2.624	Al 2.6551	Al 2.643	Al 2.6461	Al 2.6441	Al 2.6511
Vertex 6	Al 2.624	Al 2.6551	Al 2.643	Al 2.6771	Al 2.6778	Al 2.6511
Vertex 7	Al 2.883	Al 2.7521	Al 2.687	Al 2.6889	Al 2.6878	Al 2.7042
Vertex 8	Al 2.883	Al 2.7521	Al 2.687	Al 2.7061	Al 2.7127	Al 2.7042
Vertex 9	Al 2.883	Al 2.7682	Al 2.755	Al 2.7348	Al 2.7282	Al 2.736
Vertex 10	Al 2.883	Al 2.7682	Al 2.755	Al 2.8013	Al 2.793	Al 2.736
Vertex 11	Al 2.883	Nd 3.3791	Gd 3.494	Gd 3.4418	Y 3.3925	Y 3.5063
Vertex 12	Al 2.883	Nd 3.6171	Gd 3.494	Gd 3.5141	Y 3.5124	Y 3.5063
r parameter, Å	2.7535	2.8075	2.7913	2.7978	2.7927	2.7959
Volume, Å^3	52.95	56.12	55.16	55.55	55.24	55.43
Polyhedral distortion,%	0	−6.00	−4.18	−4.91	−4.33	−4.69

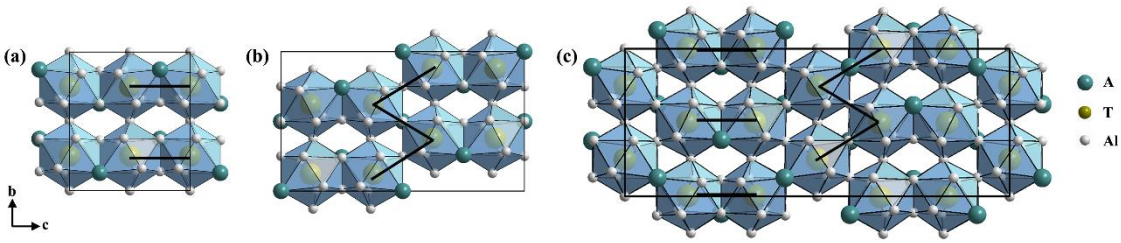

Figure 4. Chains of the interconnected icosahedrons as formed in the unit cells of three orthorhombic structures: (**a**) 1*c*, (**b**) 2*c* and (**c**) 3*c*. Parallel rows and zigzag like chains are marked by lines in (**a**) and (**b**), respectively. In (**c**) both types of connections are seen. The illustration was prepared using Diamond commercial software.

4. Conclusions

In [27,28], it was proposed that the magnetic moment of transition metal can be used for assessment of the stability of the Al-rich ternary structures forming in the A-T-Al systems, where T = 3*d* transition metal and A has either no *f* electrons or 4*f* electrons in its outer shell. In current research, a successful attempt to generalize this theory was made. CeT_2Al_{20} (T = Ta, W, Re) and YRe_2Al_{20} compositions were studied by DFT calculations in order to validate the proposed theory for compounds containing 5*d* transition metals. T = Re is a special case, since in the row of 5*d* transition metals, similar to Mn in the row of 3*d* transition metals, with this element the symmetry breaks. Generally speaking, we prove that the cubic symmetry is stable for Al-rich ternary structures forming in the A-T-Al systems (with AT_2Al_{20} composition), if is T situated in the columns 5B and 6B in periodic table while for T situated in 7B column, the symmetry breaks and less symmetric structures with AT_2Al_{10} composition crystallize. These results were compared with structural data reported in the database and found to be in excellent agreement [35]. Calculation of magnetic moments of T elements for all competing structures in each studied system allowed concluding that indeed the lowest values of the magnetic moments correspond to the stable structures obtained by total energies calculations. Analysis of DOS has shown that 4*f*-electrons peaks of A are localized above the Fermi energy level and do not contribute to the bonding with 5*d*-electrons of T. In fact, the value of magnetic moment of T atom type

imposes specific degree of distortion on coordination polyhedron formed around transition metal. Consequently, this distortion imposes specific geometry on the crystal structure formed, due to the necessity to interconnect these polyhedrons. Crystallographic analysis of distortion of coordination polyhedra, around T atoms in these systems, reasons the formation of the structural derivatives of the orthorhombic phase (referred as 1*c*, 2*c* and 3*c*) formed with T = Re. It can be seen that as a function of this distortion, sequence of the polyhedral changes-imposing larger unit cell.

Author Contributions: Conceptualization, L.M.; methodology, D.F.; validation, G.Y. and D.F.; formal analysis, D.V. and G.Y.; investigation, G.Y.; data curation, L.M. and D.F.; writing—original draft preparation, G.Y. and D.F.; writing—review and editing, L.M.; supervision, L.M. and D.F. All authors have read and agreed to the published version of the manuscript.

Funding: This research received no external funding.

Conflicts of Interest: The authors declare no conflict of interest.

References

1. Thiede, V.M.; Jeitschko, W.; Niemann, S.; Ebel, T. EuTa2Al20, Ca6W4Al43 and other compounds with CeCr2Al20 and Ho6Mo4Al43 type structures and some magnetic properties of these compounds. *J. Alloys Compd.* **1998**, *267*, 23–31. [CrossRef]
2. Thiede, V.M.T.; Ebel, T.; Jeitschko, W. Ternary aluminides LnT2Al10 (Ln=Y, La–Nd, Sm, Gd–Lu andT=Fe, Ru, Os) with YbFe2Al10 type structure and magneticproperties of the iron-containing series. *J. Mater. Chem.* **1998**, *8*, 125–130. [CrossRef]
3. Buschow, K.H.J.; van Vucht, J.H.N.; van den Hoogenhof, W.W. Note on the crystal structure of the rare earth-3*d* transition metal compounds of the type RT_4A1_8. *J. Less Common Met.* **1976**, *50*, 145–150. [CrossRef]
4. Stępień-Damm, J.; Baran, A.; Suski, W.; Stepien-Damm, J. Crystal structure of the uranium ternary compound UFe4Al8. *J. Less Common Met.* **1984**, *102*, L5–L8. [CrossRef]
5. Tamura, I.; Mizushima, T.; Isikawa, Y.; Sakurai, J. Mössbauer effect and magnetization studies of CeFe2Al8 and LaFe2Al8. *J. Magn. Magn. Mater.* **2000**, *220*, 31–38. [CrossRef]
6. Suski, W. Comparison of structure and magnetic properties of the 4f and 5f electron ThMn12-type ternary aluminides. *J. Alloys Compd.* **1995**, *223*, 237–241. [CrossRef]
7. Baran, A.; Suski, W. Magnetic properties of the UFe_nAl_{12-n} (n = 4, 5 or 6) and $ThFe_4Al_8$ intermetallic compounds. *Phys. B* **1985**, *130B*, 219–221. [CrossRef]
8. Baran, A.; Suski, W.; Mydlarz, T. MAGNETIC PROPERTIES OF THE (U, Th)(Cr, Mn)4Al8 COMPOUNDS. *Anomalous Rare Earths Actin.* **1987**, *63–64*, 196–198.
9. Steglich, F.; Stockert, O.; Wirth, S.; Geibel, C.; Yuan, H.; Kirchner, S.; Si, Q. Routes to heavy-fermion superconductivity. *J. Phys. Conf. Ser.* **2013**, *449*, 012028. [CrossRef]
10. Schafer, W.; Will, G. Neutron diffraction studies of the structural and magnetic properties of $AnFe_4Al_8$ (An=Th, U, Np) intermetallic compounds. *J. Less Common Met.* **1989**, *149*, 237–241. [CrossRef]
11. Ott, H.R. Heavy-electron metals. *Annu. Rev. Mater. Sci.* **1987**, *17*, 13–33. [CrossRef]
12. Bakker, M.; Van Dijk, A.; Wicherts, J.M. The Rules of the Game Called Psychological Science. *Perspect. Psychol. Sci.* **2012**, *7*, 543–554. [CrossRef] [PubMed]
13. Gonçalves, A.P.; Almeida, M.; Walker, C.; Ray, J.; Spirlet, J. Phase relations and single crystal growth of U-Fe-M (M = Al, Si) compounds with ThMn12-type structure. *Mater. Lett.* **1994**, *19*, 13–16. [CrossRef]
14. Cordier, G.; Czech, E.; Ochmann, H.; Schäfer, H. Neue übergangsmetallaluminide des calciums. *J. Less Common Met.* **1984**, *99*, 173–185. [CrossRef]
15. Niemann, S.; Jeitschko, W. The crystal structure of $YbFe_2Al_{10}$, a combined substitution and stacking variant of the ThMn 12 and CeMn 4 Al 8 type structures. *Z. Krist.* **1995**, *210*, 338–341. [CrossRef]
16. Kripyakevich, P.I.; Zarechnyuk, O.S. RCr2Al20 compounds in systems of rare earth metals and calcium, and their crystal structures. *Dopov. Akad. Nauk. Ukr. RSR Ser. A Fiz. Tekh.* **1968**, *30*, 364.
17. Yaniv, G.; Fuks, D.; Meshi, L. Explanation of structural differences and similarities between the AT_2Al_{10} phases (where A = actinide, lanthanide or rare earth element and T = transition metal). *Z. Krist.* **2019**, *234*, 595–603. [CrossRef]

18. Winiarski, M.; Wiendlocha, B.; Sternik, M.; Wiśniewski, P.; O'Brien, J.R.; Kaczorowski, D.; Klimczuk, T. Rattling-enhanced superconductivity in MV_2Al_{20} (M=Sc, Lu, Y) intermetallic cage compounds. *Phys. Rev. B* **2016**, *93*, 134507. [CrossRef]
19. Matsumoto, Y.; Tsujimoto, M.; Tomita, T.; Sakai, A.; Nakatsuji, S. Heavy Fermion Superconductivity in Non-magnetic Cage Compound PrV_2Al_{20}. *J. Phys. Conf. Ser.* **2016**, *683*, 12013. [CrossRef]
20. Frank, F.C.; Kasper, J.S. Complex alloy structures regarded as sphere packings. II. Analysis and classification of representative structures. *Acta Crystallogr.* **1959**, *12*, 483–499. [CrossRef]
21. Luo, H.; Krizan, J.W.; Müechler, L.; Haldolaarachchige, N.; Klimczuk, T.; Xie, W.; Fuccillo, M.; Felser, C.; Cava, R.J. A large family of filled skutterudites stabilized by electron count. *Nat. Commun.* **2015**, *6*, 6489. [CrossRef] [PubMed]
22. Stein, F.; Palm, M.; Sauthoff, G. Structure and stability of Laves phases. Part I. Critical assessment of factors controlling Laves phase stability. *Intermetallics* **2004**, *12*, 713–720. [CrossRef]
23. Winiarski, M.; Klimczuk, T. Crystal structure and low-energy Einstein mode in ErV 2 Al 20 intermetallic cage compound. *J. Solid State Chem.* **2017**, *245*, 10–16. [CrossRef]
24. Higashinaka, R.; Nakama, A.; Ando, M.; Watanabe, M.; Aoki, Y.; Sato, H. Magnetic and transport properties of YbT2Al20(T= Ti, V and Cr). *J. Physics: Conf. Ser.* **2011**, *273*, 012033. [CrossRef]
25. Namiki, T.; Nosaka, K.; Tsuchida, K.; Lei, Q.; Kanamori, R.; Nishimura, K. Magnetic and thermal properties of Nd T 2 AI 20 (T: Ti, V, Cr) single crystals. *J. Phys. Conf. Ser.* **2016**, *683*, 12017. [CrossRef]
26. Bram, A.I.; Venkert, A.; Meshi, L. Characterization of new aluminides found in the ThT 2 Al 20 alloys (where T = Ti, V, Mn). *J. Alloys Compd.* **2015**, *641*, 1–6. [CrossRef]
27. Uziel, A.; Bram, A.; Venkert, A.; Kiv, A.E.; Fuks, D.; Meshi, L. Abrupt symmetry decrease in the ThT2Al20 alloys (T = 3d transition metal). *J. Alloys Compd.* **2015**, *648*, 353–359. [CrossRef]
28. Yaniv, G.; Fuks, D.; Meshi, L. Structure and peculiarities of bonding in the Al-rich A-Mn-Al alloys (where A=Y, Gd, Th and U). *Intermetallics* **2018**, *100*, 44–51. [CrossRef]
29. Fehrmann, B.; Jeitschko, W. Lanthanoid Rhenium Aluminides with a High Content of Aluminum: LnRe2Al10(Ln = Ho−Lu) with a New Structure Type and NdRe2Al10with CaCr2Al10-Type Structure. *Inorg. Chem.* **1999**, *38*, 3344–3351. [CrossRef]
30. Fehrmann, B.; Jeitschko, W. The Intermetallic Compounds GdRe2Al10 and TbRe2Al10, Crystallizing with a Stacking Variant of the YbFe2Al10 Type Structure. *Z. Nat. B* **1999**, *54*, 1277–1282. [CrossRef]
31. Moze, O.; Tung, L.; Franse, J.; Buschow, K. Crystal structure and magnetic properties of CeV2Al20 and CeCr2Al20. *J. Alloys Compd.* **1998**, *268*, 39–41. [CrossRef]
32. Fulfer, B.W.; Haldolaarachchige, N.; Young, D.P.; Chan, J.Y. Crystal growth and magnetic properties of Ln-Mn-Al (Ln=Gd, Yb) compounds of the CaCr2Al10 and ThMn12 structure types. *J. Solid State Chem.* **2012**, *194*, 143–150. [CrossRef]
33. Fehrmann, B.; Jeitschko, W. ChemInform Abstract: The Intermetallic Compounds $GdRe_2Al_{10}$ and $TbRe_2Al_{10}$, Crystallizing with a Stacking Variant of the $YbFe_2Al_{10}$ Type Structure. *Cheminform* **2010**, *31*. [CrossRef]
34. International Center for Diffraction Data. *PDF4+ Commercial Database of the International Cneter for Diffractin Data*; ICDD: Delaware County, PA, USA, 2019.
35. Blaha, P.; Schwarz, K.; Madsen, G.; Kvasnicka, D.; Luitz, J. *WIEN2k, An Augmented Plane Wave + Local Orbitals Program for Calculating Crystal Properties*; Schwarz, K., Ed.; Technology Universitat Wien: Wien, Austria, 2001; ISBN 3- 9501031-1-2. version 10.1.
36. Desclaux, J. Hartree Fock Slater self consistent field calculations. *Comput. Phys. Commun.* **1970**, *1*, 216–222. [CrossRef]
37. Koelling, D.D.; Harmon, B.N. A technique for relativistic spin-polarised calculations. *J. Phys. C: Solid State Phys.* **1977**, *10*, 3107–3114. [CrossRef]
38. Perdew, J.P.; Burke, K.; Ernzerhof, M. Generalized Gradient Approximation Made Simple. *Phys. Rev. Lett.* **1996**, *77*, 3865–3868. [CrossRef]
39. Henderson, T.M.; Paier, J.; Scuseria, G.E. Accurate treatment of solids with the HSE screened hybrid. *Phys. Status Solidi (b)* **2010**, *248*, 767–774. [CrossRef]
40. Janesko, B.G.; Henderson, T.M.; Scuseria, G.E. Screened hybrid density functionals for solid-state chemistry and physics. *Phys. Chem. Chem. Phys.* **2008**, *11*, 443–454. [CrossRef]
41. Wang, J.; Ma, L.; Ray, A.K. On the magnetic and thermodynamic properties of Americium-II: A hybrid density functional theoretic study. *Phys. Lett. A* **2010**, *374*, 4704–4712. [CrossRef]

42. Anisimov, V.I.; Solovyev, I.V.; Korotin, M.A.; Czyyk, M.T.; Sawatzky, G.A. Density-functional theory and NiO photoemission spectra. *Phys. Rev. B* **1993**, *48*, 16929–16934. [CrossRef]
43. Antonov, V.N.; Harmon, B.N.; Antropov, V.P.; Perlov, A.Y.; Yaresko, A.N. Electronic structure and magneto-optical Kerr effect of Fe_3O_4 and Mg^{2+}- or Al^{3+}-substituted Fe_3O_4. *Phys. Rev. B* **2001**, *64*, 134410. [CrossRef]
44. Anisimov, V.; Elfimov, I.S.; Hamada, N.; Terakura, K. Charge-ordered insulating state ofFe3O4from first-principles electronic structure calculations. *Phys. Rev. B* **1996**, *54*, 4387–4390. [CrossRef] [PubMed]
45. Guss, P.; Foster, M.E.; Wong, B.M.; Doty, F.P.; Shah, K.S.; Squillante, M.R.; Shirwadkar, U.; Hawrami, R.; Tower, J.; Yuan, D. Results for aliovalent doping of CeBr3 with Ca2+. *J. Appl. Phys.* **2014**, *115*, 34908. [CrossRef]
46. Cococcioni, M.; De Gironcoli, S. Linear response approach to the calculation of the effective interaction parameters in the LDA+U method. *Phys. Rev. B* **2005**, *71*, 035105. [CrossRef]
47. Cococcioni, M. A LDA + U Study of Selected iron Compounds. Ph.D. Thesis, The university of Cambridge, Cambridge, UK, October 2002.
48. Zenou, V.; Meshi, L.; Fuks, D. Why UFexAl12−x phase does not crystallize with ThMn12-structure type, when x = 2? *Intermetallics* **2011**, *19*, 713–720. [CrossRef]
49. Zenou, V.; Rafailov, G.; Dahan, I.; Kiv, A.; Meshi, L.; Fuks, D. Ordered U(Al, Si)3 phase: Structure and bonding. *J. Alloys Compd.* **2017**, *690*, 884–889. [CrossRef]
50. Söderlind, P.; Sadigh, B.; Lordi, V.; Landa, A.; Turchi, P. Electron correlation and relativity of the 5f electrons in the U–Zr alloy system. *J. Nucl. Mater.* **2014**, *444*, 356–358. [CrossRef]
51. Xie, W.; Marianetti, C.A.; Morgan, D. Reply to "Comment on 'Correlation and relativistic effects in U metal and U-Zr alloy: Validation of ab initio approaches'". *Phys. Rev. B* **2016**, *93*, 157101. [CrossRef]
52. Söderlind, P.; Landa, A.; Perron, A.; Sadigh, B.; Heo, T.W. Ground-State and Thermodynamical Properties of Uranium Mononitride from Anharmonic First-Principles Theory. *Appl. Sci.* **2019**, *9*, 3914. [CrossRef]
53. Fuks, D.; Mastrikov, Y.; Kotomin, E.; Maier, J. Ab initio thermodynamic study of (Ba,Sr)(Co,Fe)O3 perovskite solid solutions for fuel cell applications. *J. Mater. Chem. A* **2013**, *1*, 14320. [CrossRef]
54. Murnaghan, F.D. The Compressibility of Media under Extreme Pressures. *Proc. Natl. Acad. Sci. USA* **1944**, *30*, 244–247. [CrossRef] [PubMed]
55. Thiede, V.M.; Jeitschko, W. Ternary Intermetallic Compounds LnMn2Al10 (Ln = Y, La-Nd, Sm, Gd-Dy) and LnRe2Al10 (Ln = Ce, Pr, Sm) with CaCr2Al10-Type Structure. *Z. Nat. B* **1998**, *53*, 673–678.
56. Sefat, A.S.; Bud'Ko, S.L.; Canfield, P.C. Properties of RRe_2Al_{10} (R=Y, Gd–Lu) crystals. *Phys. Rev. B* **2009**, *79*, 174429. [CrossRef]
57. Niemann, S.; Jeitschko, W. Ternary aluminide AT_2Al_{20} (A=rare earth elements and Uranium; T=Ti, Nb, Ta, Mo, and W) with $CeCr_2Al_{20}$-type structure. *J. Solid State Chem.* **1995**, *114*, 337–341. [CrossRef]
58. Kiv, A.; Ezersky, V.; Talianker, M. The stability of structures with icosahedral local order in Al-based alloys with transition metals. *Mater. Sci. Eng. A* **2003**, *352*, 100–104. [CrossRef]
59. Silberberg, M. *The Molecular Nature of Matter and Change*, 6th ed.; McGraw-Hill Science/Engineering/Math: New York, NY, USA, 2011.
60. Makovicky, E.; Balic-Zunic, T. New Measure of Distortion for Coordination Polyhedra. *Acta Crystallogr. Sect. B Struct. Sci.* **1998**, *54*, 766–773. [CrossRef]